Energy and Buildings 68 (2014) 232–241

Contents lists available at ScienceDirect

Energy and Buildings

journal homepage: www.elsevier.com/locate/enbuild

# An experimental investigation of a two-dimensional prototype of a transparent transpired collector

Messaoud Badache*, Stéphane Hallé, Daniel R. Rousse, Guillermo Quesada, Yvan Dutil

*Technologies of Energy and Energy Efficiency Industrial Research Chair (t3e), Department of Mechanical Engineering, École de Technologie Supérieure, Université du Québec 1100, Notre-Dame Street West, Montreal H3C 1K3, Canada*

ARTICLE INFO

*Article history:*
Received 20 May 2013
Received in revised form 2 September 2013
Accepted 7 September 2013

*Keywords:*
Transparent transpired solar air collector
DoE
Experimental work
Statistical analysis

ABSTRACT

This paper presents an experimental investigation of the thermal performance of a two-dimensional reduced scale prototype designed to simulate the essential features of a novel type of solar air collector involving a transparent transpired cover. Another objective is to analyze the effects of varying key parameters such as plenum thicknesses, pitch spacing, slots width, irradiation, and air mass flow rate in term of collector efficiency. A multi-level factorial design of experiments is used for this investigation. It is found that the air mass flow rate has the strongest effect on the efficiency of the transparent transpired collector. The irradiation, slots width, pitch spacing and plenum thicknesses seems to have a moderate effect.



## 1. Introduction

Solar air heating systems are becoming more and more popular as they provide many possibilities for energy savings and for preheating air in various applications. They use solar energy to heat and ventilate indoor air spaces. Implementation of these systems in new or existing buildings has been the object of a relatively broad range of applications in the last decade.

### 1.1. A new type of collector

A new type of solar collector has recently emerged on the market. It is called transpired transparent collector (hereafter TTC). The TTC includes all the usual components of a typical unglazed transpired collector (UTC). The main difference is that instead of a perforated metal absorber, a perforated glazing is used. Basically, the TTC consists of a transparent panel perforated by tiny holes, installed several centimeters (10–15 cm) from a masonry wall. A large part of the solar radiation is transmitted through the perforated glazing and absorbed by the dark surface of the building wall, namely the absorber wall. The remaining part of the incident radiation is either absorbed by the transparent cover or reflected back to the surroundings. On the top, a fan creates a negative pressure in the air space between the panel and the building wall (plenum), drawing cold air through the glazing perforations. This generates an upward air movement in the plenum. Heat collected at the absorber wall as well as part of that which is absorbed by the transparent cover itself is transferred to air that flows in the plenum, which exits from the top of the building wall. The heated air is then ducted into the building via a connection to the ventilation intake.

This type of solar collector can be installed on new and existing façades of buildings. It offers the potential advantages of low weight, simplicity of manufacturing and resistance to corrosion, as well as better aesthetic integration compared to metallic absorber. Furthermore, it can be used in conjunction with windows, overhang, double skin façade and other building design elements. A schematic of a TTC mounted on a typical brick wall construction is shown in Fig. 1. Another advantage of making the TTC as a part of the building façade is that the perforated panel can recapture building wall heat loss. As the building wall reemits the heat in the thermal infrared (~10 μm), there is not much radiative losses because the perforated glazing is almost opaque at these wavelengths. At this point, the radiation emitted by the absorber plate is absorbed at the back face of the cover and the sucked air through the perforations picks up this heat and brings it back into the plenum.

Fig. 1 shows transparent perforated panels placed in front of brick wall construction (the absorber surface), with an airspace in between, and air exhausting fan (at its top center).

*Abbreviations:* ATF, active transparent facade; UV, ultraviolet wavelength; VIS, visible wavelength; NIR, near infrared wavelength; MIR, mid infrared wavelength; FIR, far infrared wavelength.

* Corresponding author at: École de Technologie Supérieure, Mechanical Engineering Department, 1125 William Street, Montreal H3C 1P7, Canada.
Tel.: +1 514 396 8689.
*E-mail addresses:* messaoud.badache.1@ens.etsmtl.ca (M. Badache), stephane.halle@etsmtl.ca (S. Hallé), daniel.rousse@etsmtl.ca (D.R. Rousse), guillermo.quesada@etsmtl.ca (G. Quesada), yvan.dutil@etsmtl.ca (Y. Dutil).

0378-7788/$ – see front matter © 2013 Elsevier B.V. All rights reserved.
http://dx.doi.org/10.1016/j.enbuild.2013.09.010

**Nomenclature**

| | |
|---|---|
| $A_{coll}$ | collector area ($m^2$) |
| $A_{cs}$ | pipe cross section surface area ($m^2$) |
| $b$ | slot width (m) |
| $C_p$ | specific heat capacity of air (J/(kg K)) |
| $D_f$ | degree of freedom |
| $G_T$ | incident irradiation on the collector ($W/m^2$) |
| $\dot{m}$ | air mass flow rate (kg/s) |
| $L$ | pitch spacing between slots (m) |
| SST | sum of squares |
| $T_{sky}$ | sky temperature (°C) |
| $T_{amb}$ | ambient air temperature (°C) |
| $T_{out}$ | exit air temperature (°C) |
| $T_{abs}$ | average absorber wall temperature (°C) |
| $T_g$ | average perforated glazing temperature (°C) |
| $w$ | plenum thickness (m) |
| $V_{wind}$ | laboratory air velocity (m/s) |
| $k$ | number of factors with 3 levels |
| $l$ | number of factors with 2 levels |

*Greek symbols*

| | |
|---|---|
| $\rho_{air}$ | air density ($kg/m^3$) |
| $\lambda$ | thermal conductivity (W/m·K) |
| $\eta_{coll}$ | collector efficiency |
| $\tau_g$ | transmissivity of perforated glazing |
| $\rho_g$ | reflectivity of perforated glazing |
| $\tau_{ir,g}$ | thermal infrared transmissivity of perforated glazing |
| $\alpha_{abs}$ | the total hemispherical absorptivity of absorber plate |
| $\varepsilon_{abs}$ | thermal emissivity of the absorber plate |

### 1.2. A transparent cover

The use of polymers in the design of solar collector systems is not new concept, there is a relatively long history on their utilization [1]. A number of researchers have adopted the use of polymers in solar collector design [2]. Two of the earliest reports on the use of polymer materials in solar collector systems were by Tabor and Zeimer [3] and Whillier [4]. Tabor and Zeimer [3] tested a cylindrical concentrator made of inflated polymer films, for the production of industrial process heat. A review of candidate materials is provided in [5]. Plastics of thicknesses from 0.5 mm to 3.2 mm are used as cover in solar collectors. These plastics have a transmission coefficient for short wave radiation that varies from 0.89 to 0.97 [6]. The thermal behavior of a polymeric solar collector for heating air has been investigated by Njomo [7,8]. Solar optical properties of a polymeric cover material are an important parameter that affects the amount of solar energy absorbed by a solar collector. Polymeric covers for solar collector with black absorber have to be selective in the solar and infrared wavelength range. A good cover material should have a high transmittance in the visible range of the electromagnetic spectrum and a low transmittance to infra-red radiation in order to trap efectively the re-radiated heat from the absorber plate [9]. The solar optical properties of such materials have been investigated in depth by Balocco et al. [10] and Oreski et al. [11,12]. The use of polymeric cover in solar collectors is preconditioned by their durability and weatherability. The details of their reliability, durability and long-term performance have been reported by Raman et al. [5] and Köhl et al. [13]. The effects of environmental variables on the performance properties of polymeric materials are reported in reference [14].

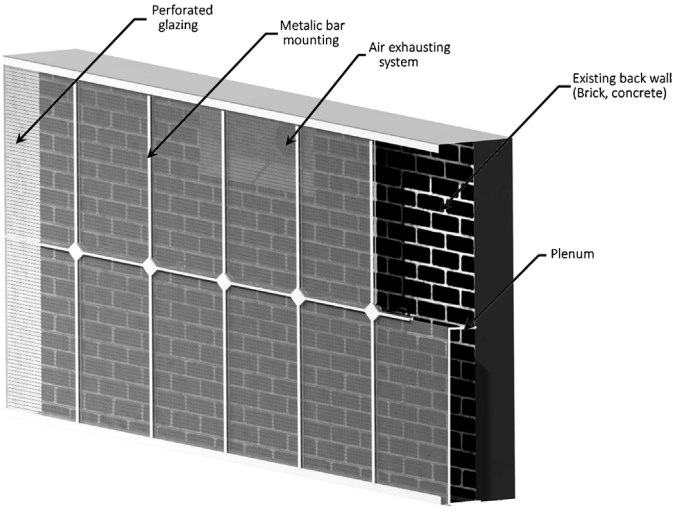


**Fig. 1.** Schematic of the transparent transpired collector mounted on a typical brick wall construction.

### 1.3. The performance of a TTC

The air passage through the TTC perforations forms tiny jets exiting the transparent perforated glazing. These jets disturb the vertical flow in the plenum and give birth to various coupled thermal (conduction, convection and radiation) and aerodynamic phenomena. The thermal performance and the specific temperatures ($T_g$, $T_{abs}$, $T_{out}$) of the various TTC components are the result of these phenomena which depend on design; thermo-physical and optical properties; and operating conditions of the various components of the TTC structure, environmental conditions and of the building itself. Table 1 summarizes the parameters affecting the performance of TTCs. This table presents the parameters classified in geometric, thermo-physical, optical and operating parameters.

The performance of a TTC depends on many parameters (Table 1) for which the influence has to be determined. Without this knowledge, an inadequate design could result. The overall performance could then be inconvenient leading to:

- Significant solar gains possibly overheating the buildings during summer time.
- Poor flow distribution across the whole system, which causes hot spots, where the radiative losses will dominate.
- Reversal flow due to natural convection, in which the air drawn into the plenum is expelled outdoor at the top of the unit.
- Significant thermal heat loss, resulting from poor optical solar and infrared properties of the TTC surface components.

The proper knowledge of the influence of each parameter enables one to increase the heat recovery, reduce costs or adapt their design to a particular context. To the best of the knowledge of the authors, no study has been published on the evaluation of the thermal performance of the TTCs as well as the main parameters that affect the performance in these devices. Therefore, it is essential to conduct a detailed research in this area.

The objective of the work presented here is to provide measurements from a reduced-scale prototype that can be used to estimate the thermal performance of TTCs and to determine the effect of some design and operation parameters such as geometrical properties, irradiation, and air mass flow rate in terms of collector efficiency ($\eta_{coll}$). To determine these parameters effects, this experimental work uses a multi level full factorial plan of replicated 48 tests. No attempt was made to derive an overall efficiency model for this collector.

**Table 1**
Parameters affecting the performance of TTC.

| Geometric | Thermo-physical | Optical | Operating conditions |
|---|---|---|---|
| Hole diameter, pitch spacing, plenum thickness, thickness of glazing, height of the collector, arrangement of holes, porosity | Thermal conductivity ($\lambda_g$, $\lambda_{abs}$), heat capacity ($c_{p,g}$, $c_{p,abs}$) | Solar and thermal properties of the TTC surface components ($\varepsilon_{abs}$, $\alpha_{abs}$), ($\rho_g$, $\tau_g$, $\alpha_g$, $\varepsilon_g$), refractive index and the extinction coefficients of the transparent cover | Air mass flow rate, incident solar incidence angles, $T_{amb}$, $V_{wind}$, wind direction, and $T_{sky}$, pressure drop through glazing, pressure drop through plenum |

In the following sections, the design of experiments methodology applied to a specific TTC is presented. A brief description of the elements that enter into the composition of experimental set-up, and the experimental procedure is provided in Section 3. The results and a discussion of the parameters effects and their interactions are reported in Section 4. The paper ends with the conclusions, which are stated in Section 5.

## 2. Design of experiment (DoE)

This section presents the design of experiments (DoE) methodology for which the objective is to estimate and compare the direct and combined effects of the investigated parameters. There are many plans that can be used to achieve this objective. Here, the factorial design of experiments is employed: it is the simplest and most widely used. Recall briefly, that the method has been the object of an extensive literature [15–17], and has been specifically used in the field of transpired solar air collectors by Badache et al. [18] and Gawlick et al. [19]. A chart of the various steps that should be followed is provided in references [20–22].

### 2.1. Selection of parameters and their levels

The first step in the construction of an experimental design is to select the various parameters and their range of variation (denoted levels 1, 0, and −1, respectively) to define the nature and number of experiments. Referring to previous works performed on similar systems [2], double-skin façade [23], active transparent façade [24], and UTCs [18,19,25] indicated that twenty-three parameters in particular were likely to have at least some impact on the performance of a TTC (Table 1).

A preliminary study was then conducted to ensure that the most relevant parameters would be selected and that their intervals generate a significant variation on the response parameter. All intervals of variation of parameters collectively define the experimental domain.

Since there is a great diversity of parameters involved, it was practically impossible to provide a DoE for such a system (with twenty-three parameters). Therefore, parameters selection was chosen with respect to three limitations. First, the sensitivity limitation; when one of these parameters is found to have a low sensitivity (perforated glazing plate thickness), it is replaced by another parameter more sensible in additional factorial runs. The second limitation is imposed by the material constraints and time which led us to fix various control parameters, such as the nature of the perforated glazing. Note that, first tests were carried out with two type of glazing material, polyethylene terephthalate glycol (PETG) and polycarbonate (PC). The difference between PETG and PC was found not to be significant. The third limitation is imposed by the choice of conducting tests in a controlled environment, which allowed to fix some parameters such as incidence angles, $T_{amb}$, $V_{wind}$, wind direction, and $T_{sky}$.

After a preliminary study, five parameters have been identified as most relevant. These parameters are: (1) the plenum thickness ($w$), (2) the pitch spacing ($L$), (3) the slots width ($b$), (4) the air mass flow rate ($\dot{m}$), and (5) the incident solar radiation ($G_T$).

Here, one should be aware that the transparent cover perforations were horizontal slots instead of traditional holes. The rationale behind this choice lies in the interest to obtain a

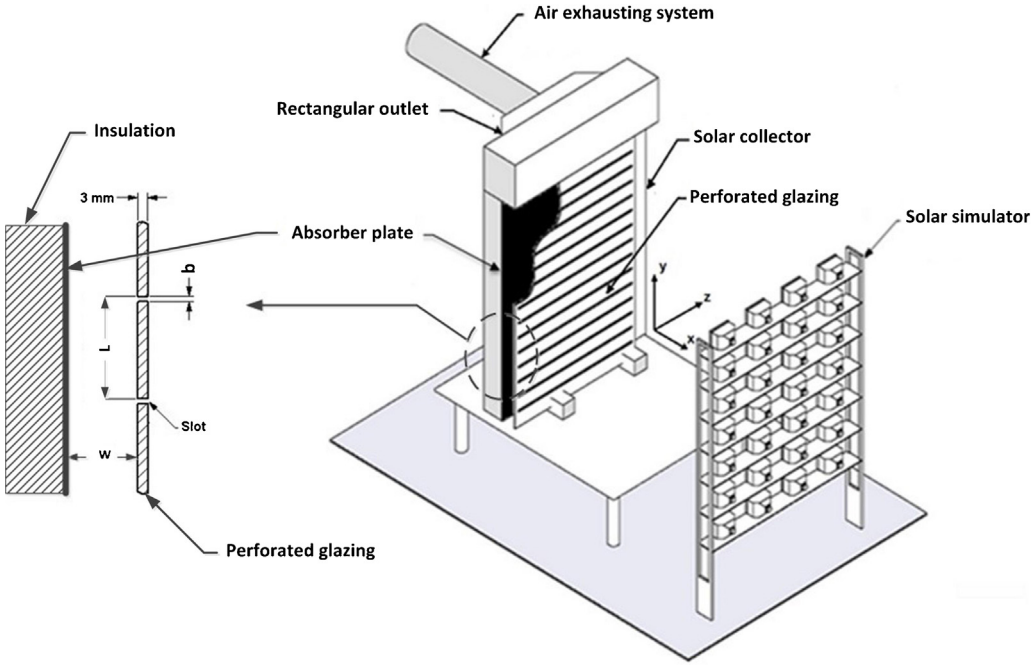


**Fig. 2.** Schematic of the experimental apparatus.

**Table 2**
Parameters and their levels used in DoE.

| Symbol | Factors | Unit | Levels of factors | | |
|---|---|---|---|---|---|
| | | | Low (−1) | Inter (0) | High (1) |
| A | Slots width ($b$) | m | 0.001 | – | 0.002 |
| B | Plenum thicknesses ($w$) | m | 0.05 | – | 0.15 |
| C | Pitch spacing ($L$) | m | 0.02 | – | 0.03 |
| D | Irradiation ($G_T$) | W/m$^2$ | 300 | – | 600 |
| E | Mass flow rate ($\dot{m}$) | kg/s | $2.2 \times 10^{-3}$ | $4.2 \times 10^{-3}$ | $6.3 \times 10^{-3}$ |

two-dimensional representation of a three-dimensional collector. This is to ease the upcoming implementation of a numerical model to simulate the whole collector in the vertical mid-plane (Fig. 2).

The preliminary tests have also allowed to identify, for each parameter studied, the range of values (high, medium and low), used to develop the DoE plan. Table 2 summarizes the selected parameters and their levels used in DoE.

During the construction of the DoE, the experimental domain of parameters was chosen as wide as possible, since no previous published results for TTCs were available as a starting point. For slot's width ($b$), three levels were selected at first. However, because the preliminary tests have shown that the effect of the slots width on efficiency is almost linear, only two levels were kept. Slots were made into the polycarbonate plate with an accuracy of ±0.1 mm using a laser. Slots width values selected were 0.001 and 0.002 m by analogy with the UTCs. Incident irradiation was constrained by the maximum intensity of our radiative heat source. The values of the lowest and the highest level considered for $G_T$ were 300 W/m$^2$, and 600 W/m$^2$ respectively. The choice of three levels for mass flow rate was motivated by the fact that it is a very important parameter, and the need for an accurate representation of this factor in the DoE investigation. The mass flow rates values used were $2.2 \times 10^{-3}$, $4.2 \times 10^{-3}$, and $6.3 \times 10^{-3}$ kg/s which correspond to unit mass fluxes of $1.45 \times 10^{-2}$, $2.72 \times 10^{-2}$, and $4.10 \times 10^{-2}$ kg/(m$^2$ s). These values spanned the range of practical mass flow rate studied in UTCs [26]. For the pitch spacing and the plenum thickness, two levels were used and the variation of efficiency with respect to these two parameters levels was assumed to be linear. Their respective values were 0.02 and 0.03 m for pitch, and 0.05 and 0.15 m for the plenum thickness.

On the other hand, the efficiency of the TTC was selected as the response parameter which could be used to estimate and compare the effects of variations within the parameters experimental domain. Several studies in the literature [27,19] considered the efficiency ($\eta_{coll}$) as the relevant indicator of the thermal performance of solar air collectors. $\eta_{coll}$ was defined as the product of the air mass flow rate ($\dot{m}$), the specific heat of air ($C_p$) and the air temperature increase between collector inlet and outlet ($T_{out} - T_{amb}$) divided by the irradiation ($G_T$) times the collector area ($A_{coll}$) (Eq. (1)). No attempt was made to derive a physical model to predict the value of $\eta_{coll}$ for this collector.

$$\eta_{coll} = \frac{\dot{m} C_p (T_{out} - T_{amb})}{G_T A_{coll}} \quad (1)$$

### 2.2. Planning matrix

The number of experiments ($N$) required for all combinations can be calculated with Eq. (2) [20,21]:

$$N = 3^k \times 2^l \quad (2)$$

where $k$ is the number of factors with 3 levels and $l$ is the number of factors with 2 levels of variation. According to Table 2 and Eq. (2), the number of tests of the factorial plan corresponds to $3^1 \times 2^4 = 48$.

It was not possible to perform a fractional factorial plan to reduce the number of tests, because the analysis of interactions is more difficult, and the interactions are often factors combined with simple or higher order interactions. Given the probability of the presence and the importance of studying such interactions, it was decided to keep a full factorial plan even if a high number of tests had to be performed. The study of a comprehensive multi-level plan is to consider all possible combinations of the factors considered in the analysis [28]. Second and higher order interactions were assumed negligible, since their interpretation is not obvious. Tests were conducted following a preselected order due to practical constraints. Theoretically, proceeding in that way is disputable, because tests plans should comply with basic principles of randomization [22]. However, we had the opportunity to carry out a second series of 48 tests that are identical to the first 48 tests, and these have been added to the DoE.

## 3. Experimental set-up and procedure

The experimental apparatus is schematically depicted in Fig. 2. This experimental apparatus involves three main parts: the transparent transpired collector; the air exhausting system; and the solar simulator.

The transparent transpired collector is 0.32 m width (in $z$), 0.60 m height (in $y$), and includes a variable plenum thickness ($w$) (in $x$). It involves a glazing with slots (acting as a cover and called 'perforated glazing' in the rest of this paper), and a vertical wooden box, which, itself involves the back wall (1.9 cm thick plywood) and sides. The back wall is fitted with a rectangular outlet opening fixed at its top center. The inner face of the wooden box (back wall) was covered by an aluminum metal sheet 'absorber plate' (painted with selective black coating). The exterior face and sides of the box were insulated with 10 cm thick polystyrene, and reinforced with a layer of 0.5 cm thick of thermo-foil. The adiabatic conditions for the insulated walls were verified during the test runs in which the maximum heat loss through the back wall and sides did not exceeded 1 W for the entire insulated surface of the collector. The relevant absorber plate surface thermo-optical properties are $\varepsilon_{abs} = 0.52$ and $\alpha_{abs} = 0.96$, which were taken from Thurmalox® 250 selective black coating technical data sheet.

The plenum level was varied by increasing the thickness ($w$) from 0.05 m to 0.15 m. More information on the manner in which its level has been changed is described in previous work [25].

The air exhausting system and the solar simulator developed in previous work [18] were used in this study. No significant modifications have been made. The solar simulator allows obtaining two levels of irradiation 300 and 600 W/m$^2$ within ±3% uniformity. The air suction system provides the three air mass flow rates required in the experiments ($2.2 \times 10^{-3}$, $4.2 \times 10^{-3}$, $6.3 \times 10^{-3}$ kg/s).

The perforated glazing material under study is polycarbonate (PC). This choice is justified by its widespread application as a glazing material for solar applications [29,30]. The relevant spectral optical properties of PC have been measured before lamps exposure and are displayed in Fig. 3 following the procedure explained below.

According to the properties listed in Table 2, four rectangular perforated glazing test plates of dimension 0.003 m thick by

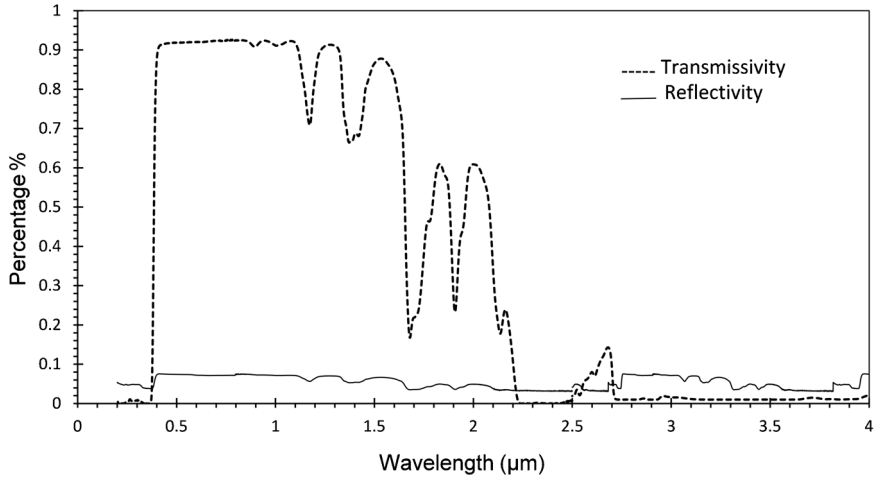


**Fig. 3.** Normal transmissivity and reflectivity, spectra for PC (0.003 m thick).

0.32 m wide by 0.48 m height were tested. For upcoming calculation of the efficiency, the effective surface area of the collector is $A_{coll} = 0.154\ m^2$. Each test plate includes an equally spaced single row of slots, and characterized by the width of the slots ($b$), the pitch spacing ($L$). The perforated glazing includes 21 slots for $L = 0.02$ m, and 15 slots for $L = 0.03$ m.

### 3.1. Measurements

The experimental setup was instrumented for the measurement of the amount of irradiation ($G_T$) incident on the collector, ambient ($T_{amb}$) and collector outlet air temperatures ($T_{out}$), temperature of absorber plate ($T_{abs}$), and perforated glazing ($T_g$), air mass flow rate at the exit off the duct ventilator ($\dot{m}$), and laboratory air velocity ($V_{wind}$). The spectral optical properties were measured with two different spectrometers presented later in the paper. The thermo-physical properties of air ($C_p$, $\rho_{air}$,) employed in the calculation of the efficiency and the air mass flow rates were taken from available standard tables in Incropera et al. [31] corresponding to mean outlet air temperature $T_{out}$. Furthermore, the effect of humidity on thermo-physical properties has been assumed negligible since the change in relative humidity values during experimentations was less than 10%. The tests were conducted in essentially still air, the measured laboratory air velocity ($V_{wind}$) was between 0.10 and 0.15 m/s.

#### 3.1.1. Measurements of temperature

Seventeen calibrated k-type thin thermocouples (0.2 mm diameter with an uncertainty of ±0.3 °C) were implemented at different positions for temperature measurements. Four thermocouples were inserted at the vertical centre-line along the height of the absorber plate ($y$-axis in Fig. 2), and four others inserted at similar positions on the perforated glazing plate. Two thermocouples measured the temperatures of the rear part of the collector (part insulated and not exposed to lamps irradiation) to estimate the heat losses through the back wall and sides. Four thermocouples measured ambient air temperature. One of them located in front of the collector and placed centrally inside a lightweight radiation shields to reduce, as far as possible, any effects of lamps radiation. The others thermocouples were located behind the collector. Three other thermocouples measured the outlet air temperature ($T_{out}$) at the exhaust pipe before the fan. Each thermocouple in place was calibrated between 0 and 50 °C.

To determine the real surface temperature of PC, measurements have been corrected with the method described in Trombe and Moreau [32].

#### 3.1.2. Measurements of mass flow rate

To determine the mass flow rate, the average air velocity ($\bar{V}$) inside the exhaust pipe is measured in five positions by a hot wire anemometer (TSI, VELOCICALC Model 9545) with a reading uncertainty of 3% or ±0.015 m/s, whichever is greater. The average air velocity is multiplied by the air density $\rho_{air}$ and by the pipe cross sectional area $A_{cs}$ and then divided by the collector area ($A_{coll}$).

The uncertainty of these measurements is taken as $\Delta\bar{V}/\bar{V} = 0.03$. The uncertainty for $\rho_{air}$ is assumed to be $\Delta\rho_{air}/\rho_{air} = 0.02$ for a total uncertainty of the mass flow rate equal to $\Delta\dot{m}/\dot{m} = 0.04$.

#### 3.1.3. Measurements of solar and radiative properties of polycarbonate

Accounting for radiative heat transfer within TTCs requires knowledge of the solar and radiative properties of PC material, namely the transmissivity ($\tau$), the absorptivity ($\alpha$), and the reflectivity ($\rho$). These properties vary with wavelength. Therefore, the aforementioned properties data were determined using two experimental apparatus. Over UV/VIS/NIR range from 0.175 to 2.5 μm the transmissivity and reflectivity spectra at normal incidence measurements were carried out using a CARRY 5000 UV/VIS/NIR spectrophotometer with an uncertainty of 0.1% for UV–vis range and 0.4% for NIR range. The mid and far infrared (2.5–25 μm) range measurements were obtained with a Fourier transform infrared spectrometer (Nicolet 6700 spectrometer) with a spectral resolution of 0.125 $cm^{-1}$. The transmissivity and reflectivity spectra are shown for 0.003 m thick PC sheets (Fig. 3).

As we can see in Fig. 3, the polycarbonate is entirely opaque at UV region (0.175–0.38 μm) and has a variable transmissivity both in the solar and in the NIR spectrum (0.38–2.2 μm). While at infrared wavelengths longer than 2.2 μm, the transmissivity drops very close to zero, and it remains the same until 25 μm (range 4–25 μm not represented). Fig. 3 shows also that the reflectivity is less than a 10% across the entire spectrum (0.175–25 μm).

### 3.2. Test procedure and initial observations

A typical test run has been performed in the following manner. The perforated glazing plate under test was mounted on the front face of the wooden box, and the plenum thickness was set to the corresponding value 0.05 m or 0.15 m. The mass flow rate was adjusted to the required values $2.2 \times 10^{-3}$ kg/s, $4.2 \times 10^{-3}$ kg/s, and $6.3 \times 10^{-3}$ kg/s. The solar simulator was switched on, and the irradiation was adjusted (using a pyranometer type CMP11 from Kipp and Zonen) to a constant value during the test period. Measurements took typically 3–4 h to achieve steady state conditions,

during which the ambient temperature varied by no more than 2 °C. The temperatures were recorded at fixed time intervals of 1 s, using a data acquisition module. The heated air (at temperature $T_{out}$), collected through the exhaust pipe, constitutes the useful heat gain that is employed to estimate the collector efficiency as reported in Eq. (1).

The following initials observations were made:

- The ambient temperature at the position closest to the front face of the TTC was higher (1–1.5 °C) than those recorded at further positions. Laboratory ambient temperature generally ranged from 25 °C to 27 °C. The temperature of the air entering the TTC is taken as the ambient air temperature at front collector.
- The perforated glazing temperature ($T_g$) was naturally greater than the laboratory air temperature ($T_{amb}$) but less than the absorber plate temperature ($T_{abs}$). This confirms that the perforated glazing material absorbs some radiation. Refs. [33,34] also noticed this trend, but for flat plat collectors. They attributed it to radiation heat losses from the absorber plate to the cover. Sandberg and Moshfegh [35] reported that as much as 40% of the heat absorbed in a solar collector can be transferred by radiation from the absorber plate to the cover. In this study, a part of this trend may also be attributed to the source light used in the experiments since its spectral distribution is slightly shifted to the infrared compared to the solar irradiation, as its maximum emission occurs at wavelength value of 0.97 μm while that of the Sun is at 0.50 μm. Finally, PC is not perfectly transparent to radiation in the 0.50–0.97 μm range as shown in Fig. 3.
- Temperatures at the highest position of the absorber plate ($T_{abs}$) and the perforated glazing ($T_g$) were higher than the temperatures below them, i.e., the temperature is increasing with $y$ (towards the top of the TTC). Collector temperatures ($T_{abs}$) and ($T_g$) become progressively more uniform as the air mass flow rate increases. Therefore, their corresponding values are taken as the mean of the measured temperatures at four different locations on the absorber plate and the perforated glazing, respectively.
- The temperature difference between the rear part of the collector and the ambient of the laboratory ($T_{amb}$) does not exceed 0.5 °C. Taking into account a heat transfer coefficient by natural convection of 8 W/m$^2$ K and a rear part surface area of 0.25 m$^2$, the heat losses through this part are generally less than 1 W. This confirms the hypothesis of considering back wall adiabatic conditions.

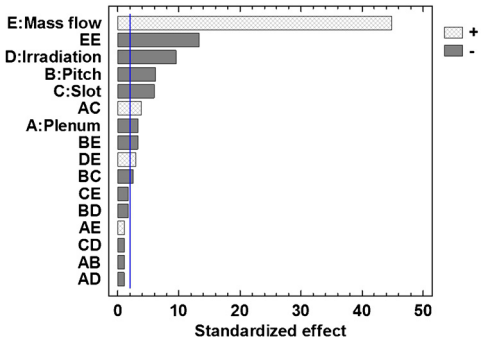


**Fig. 4.** Pareto diagram of the efficiency of the TTC.

## 4. Results and discussion

Based on parameters listed in Table 2 and using analysis software Statgraphics Centurion XV [36], a multi-level factorial design containing a replicated 48 experimental tests has been constructed. The results are summarized in this section with a detailed discussion of all parameters effects as well as their interactions based on a 5% degree of significance.

To determine whether or not the studied parameters (eventually their interactions) have a significant effect on the efficiency, an analysis of variance (ANOVA) was performed on the basis of the aforementioned experimental results (96 response output values of the efficiency). The ANOVA subdivides the total variation of the efficiency into meaningful components associated with the selected sources of variation. It also enables to obtain an estimate of the variances attributable to these sources of variation. The results of the analysis are displayed in Table 3. Small $p$-values (less than 0.05 for a significance level of 5%) correspond to significant parameters effects. For $p$-values greater than 0.05, the experiment did not detect differences between factor levels. More definition of ANOVA table columns are provided in [18]. Reading Table 3, all of the main effects are statistically significant as is the interaction between A × C, B × C, D × E, and B × E. In total, there are ten statistically significant effects.

The Pareto diagram (Fig. 4) provides the influential factors in order of decreasing contribution. The vertical line in the Pareto diagram indicates the statistical significance at 95% of confidence level and separates factors that are significant to those that are not. The Pareto diagram shows the predominance of mass flow rate

**Table 3**
Analysis of variance for the efficiency of the TTC.

| Source | Sum of squares | Df | Mean square | *F*-Ratio | *P*-Value |
|---|---|---|---|---|---|
| A: Plenum | 77.85 | 1 | 77.85 | 11.05 | 0.0014 |
| B: Pitch | 271.05 | 1 | 271.05 | 38.48 | 0.0000 |
| C: Slot | 251.65 | 1 | 251.65 | 35.73 | 0.0000 |
| D: Irradiation | 635.97 | 1 | 635.97 | 90.30 | 0.0000 |
| E: Mass flow rate | 14189.60 | 1 | 14189.60 | 2014.65 | 0.0000 |
| A × B | 8.81 | 1 | 8.81 | 1.25 | 0.2667 |
| A × C | 104.73 | 1 | 104.73 | 14.87 | 0.0002 |
| A × D | 7.36 | 1 | 7.368 | 1.05 | 0.3097 |
| A × E | 9.27 | 1 | 9.27 | 1.32 | 0.2547 |
| B × C | 46.30 | 1 | 46.30 | 6.57 | 0.0123 |
| B × D | 20.21 | 1 | 20.21 | 2.87 | 0.0942 |
| B × E | 76.65 | 1 | 76.65 | 10.88 | 0.0015 |
| C × D | 8.83 | 1 | 8.83 | 1.25 | 0.2660 |
| C × E | 20.29 | 1 | 20.29 | 2.88 | 0.0936 |
| D × E | 63.16 | 1 | 63.16 | 8.97 | 0.0037 |
| E × E | 1253.89 | 1 | 1253.89 | 178.03 | 0.0000 |
| Blocks | 16.35 | 1 | 16.35 | 2.32 | 0.1315 |
| Total error | 549.36 | 78 | 7.04 | | |
| Total (corr.) | 17611.40 | 95 | | | |

**Table 4**
Effects of parameters.

| Parameters | Plenum thickness | Pitch spacing | Slot width | Irradiation | Mass flow rate | A × C | B × C | B × E | D × E | E × E |
|---|---|---|---|---|---|---|---|---|---|---|
| Effect | −0.90 | −1.68 | −1.61 | −2.57 | 14.89 | 1.04 | −0.69 | −1.09 | 0.99 | −7.66 |

(factor E). As expected for previous work on UTCs, the mass flow rate (factor E) has the greatest effect on efficiency. Next in order of importance is irradiation (D), pitch spacing (B), slots width (C), and the less influential parameter is the plenum thickness (A). The interaction effects are in the following order; (1) interaction between plenum thickness and slot width (A × C); (2) interaction between pitch spacing and mass flow rate (B × E); (3) interaction between irradiation and mass flow rate (D × E); (4) interaction between pitch spacing and slot width (B × C).

Table 4 summarizes the values of the aforementioned significant parameters effects calculated with Statgraphics tools. The calculated value reported in Table 4 has a negative value when the increase of the parameter results in a decrease of the efficiency. This is the case for all but one (flow rate) parameters. This is shown to be the case for the principal interactions too.

All factors and interactions effects are discussed in the next subsections.

### 4.1. Main factors effects on the efficiency

A plot of the main effects of the selected factors on the efficiency is shown in Fig. 5. The main effect of each factor is defined as the difference between the average of the efficiency on the higher (1) and the lower (−1) level. Again, the mass flow rate is found to be the factor that has the biggest impact on the efficiency. This confirms our initial observations on the effects given by the Pareto diagram (Fig. 4).

- Mass flow rate effect

The effect of mass flow rate on efficiency is obvious in Fig. 5 (curve E). Unlike the others factors, efficiency increases with the mass flow rate. This trend is not surprising since high mass flow rate will induce higher velocities and which in turn improve the heat transfer from the absorber plate and the perforated glazing to the air and consequently reduce the heat losses.

A slight non-monotonic evolution of the efficiency is also observed for this effect, which is due to the presence of the quadratic effect term (E × E) in Eq. (3) ($\eta_{coll} = f(\dot{m})$). The uncertainty on the efficiency (Eq. (3)) is evaluated at ±5%. Note this equation describes the change in efficiency when air mass flow ranging between its low level (−1) to its high level (1), with all other factors held constant at 0. A relatively high value of E × E = −7.66, results in a high curve slope ($d\eta_{coll}/d\dot{m} = 14.89 - 15.32\dot{m}$). In consequence, the efficiency curve is almost linear in the range of variation of $\dot{m}$ ($2.2 \times 10^{-3}$–$6.3 \times 10^{-3}$ kg/s).

$$\eta_{coll} = 80.31 + 14.89\dot{m} - 7.66\dot{m}^2 \quad (3)$$

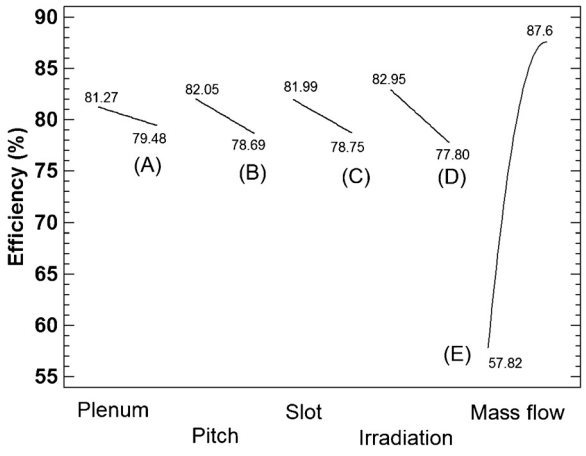


**Fig. 5.** Plots of main factors effects on the efficiency of the TTC.

- Irradiation effect

Increasing irradiation has a negative effect on the collector efficiency. In this case, higher efficiencies are obtained at low irradiation levels. The main effect for irradiation is −2.57%. This slight effect can be explained by the fact that, the equilibrium temperature of the perforated glazing and the absorber increases with increasing irradiation level. This increases the radiative heat losses from the TTC to the surroundings.

Here, one should note that although the efficiency may slightly decrease with increasing irradiation, the augmentation of $G_T$ will nevertheless increase the amount of energy recovered by the collector.

In the present study, the main source of heat loss in the TTC occurs on the perforated glazing exposed surface. Convection loses should be negligible, because tests were carried out in laboratory condition under slight air movement. Radiation losses will be dominant and may be divided into two parts: (1) losses from the absorber plate, and (2) losses from the perforated glazing. The losses by the absorber plate are mainly by conduction through the back wall and by emitted radiation to the cover plate and reflected solar radiation that has not been absorbed by the wall itself. On the other hand, the losses from the perforated glazing are mainly due to emitted radiation to the surroundings, reflected solar radiation. Thus, when the irradiation increases, the surfaces collector temperature (absorber plate and perforated glazing) are higher, the overall radiative heat losses to the surrounding increases which leads to this slight drop in efficiency.

- Pitch spacing and slots width effect

Fig. 5 (curve B) and 5 (curve C) show the effect of pitch spacing (factor B) and the slot width (factor C) on the efficiency. Changing the pitch spacing and the slot width between their low and high level, results in a drop of 3.36% and 3.24% in the efficiency (i.e. their main effects are −1.68% and −1.61% respectively). These small effects due to slot width and the pitch spacing on efficiency suggests that not much heat transfer can occur through the perforated glazing plate, and implies that the majority of heat transfer occurs at the absorber plate.

For a fixed mass flow rate, increasing the slot with makes the local air velocity lower at the exit of the slots. The vertical flow in the plenum and the thermal boundary layer on the absorber plate are less disturbed resulting to a lower heat transfer at the back plate. Similar observations, performed on black aluminum front plates, have been made by previous workers [19,37].

Fig. 5, curve B, shows that the highest efficiency is obtained at low values of the pitch spacing. This is probably due to the fact that, the glazing temperature for a large spacing is slightly higher than the temperature reached for a small spacing. Heat is transferred from the glazing to the air drawn to the plenum. Thus, small spacing

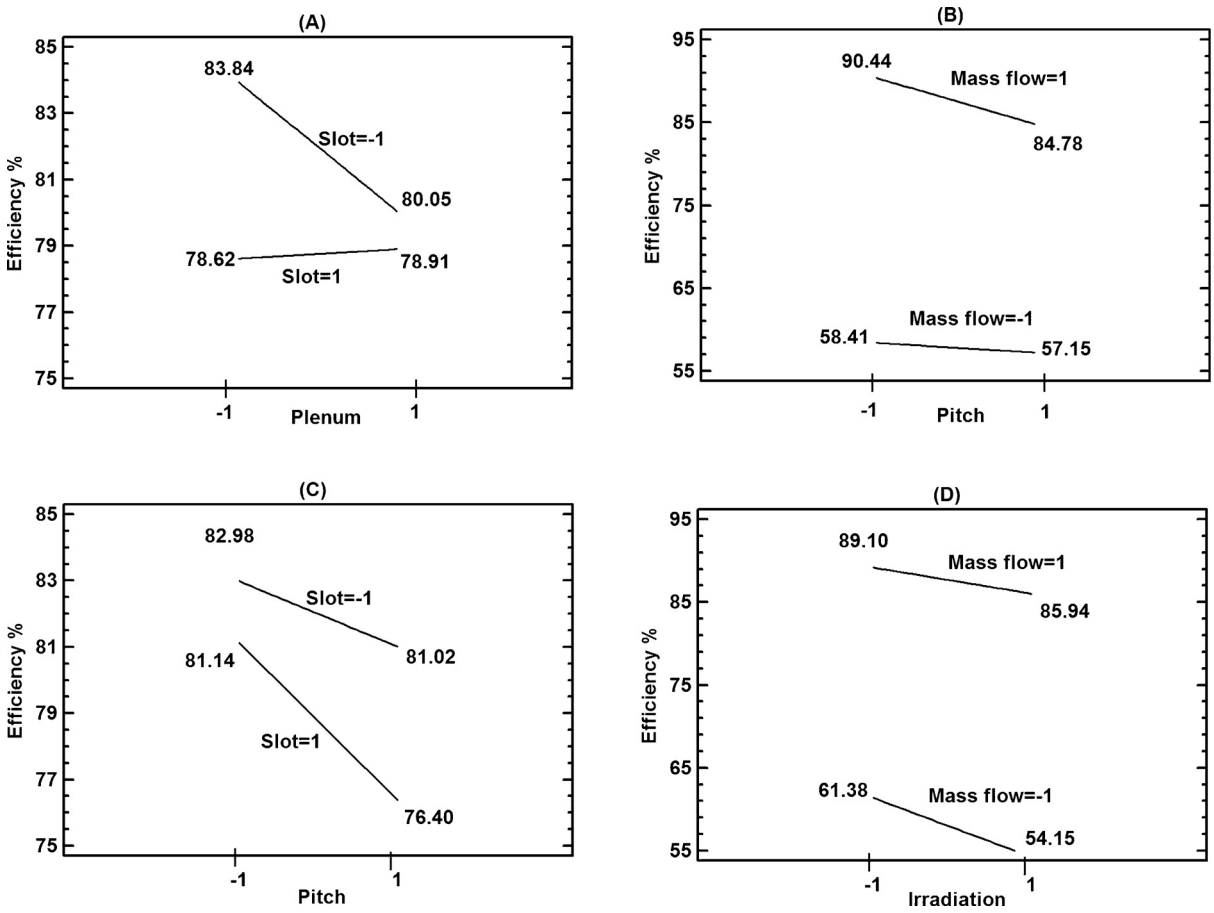


**Fig. 6.** Interactions effects of the principal parameters on the efficiency of the TTC.

results in lower glazing temperature and lower radiative heat losses and consequently in higher collector efficiency.

• Plenum effect

Fig. 5, curve A, highlights the effect of plenum thickness (factor A). The effect of this parameter is slightly negative (−0.90%), which means that when the plenum thickness increases from 0.05 to 0.15 m, the collector efficiency decreases by 1.79%. Njomo [8] and Choudhury and Garg [27] showed similar trends for unglazed opaque collectors. This effect can be attributed to the fact that higher flow velocities are induced in the plenum with reduced thicknesses. The average air vertical velocity in the narrow plenum is three times greater than that for the large plenum. This obviously causes larger heat transfer coefficients from the absorber plate to the vertical air flow, and results in higher efficiencies of the TTC. Contrary to what was expected, the efficiency is only slightly dependent of the thickness of the plenum. This may be due to the fact that the thermal boundary layer on the absorber plate and the perforated glazing are not fully developed. Moreover, in both cases though, the jets created at the exit of the slots never reach the absorber plate and could explain the insignificant differences. Experimental and numerical investigations must be undertaken in the future using TTC's plenums with larger heights to assess the effect of this factor.

It is relevant to note that the plenum thickness is a parameter which is mostly determined or dictated by manufacturing rather than thermal considerations.

### 4.2. Interactions between factors

An interaction is present between two parameters when the effect of one parameter changes over the levels of another parameter. The interactions effects on the efficiency of the TTC are depicted in Fig. 6(A)–(D) by the presence of nonparallel lines.

In each figure, efficiency is reported for two thresholds for the main investigated parameter and two curves (straight lines here) are provided for the variation of the other parameter.

The strongest interaction is between factors (A) and (C), i.e. the interaction (A × C) (Fig. 6 (A)). Interaction between others factors, (B × E), (D × E), and (B × C), is much weaker. In consequence, the lines are almost parallel.

• Interactions between plenum thickness and slot width (A × C)

For a plenum thickness of 0.05 m, Fig. 6(A) shows that changing the slot width from its high level (1) to its low level (−1), increases the efficiency from 78.62% to 83.94%, i.e. an increase of 5.32%. However, an increase of only 1.15% is observed for high (1) plenum thickness. This means that the slot width effects are not constant across plenum thickness levels (the interaction effect between plenum thickness and slot width is determined as [(−5.32%) − (−1.15%)]/4 = −1.04%). Hence, the slot width has a larger effect on the efficiency of the TTC having a small plenum thickness, than that having a larger plenum thickness. This can be explained by the fact that air jet flows discharged from smaller slots width penetrate deeper into the plenum than that of a larger slot, and the air flow in the plenum 0.05 m is more disturbed (turbulent)

than that of plenum of 0.15 m, which results in better heat transfer from the absorber plate, and therefore, in a higher efficiency of the TTC.

- Interactions between pitch spacing and mass flow rate (B × E)

The interaction effect plot in Fig. 6(B) shows how the effect (on the efficiency) of mass flow rate is decomposed through the levels of the pitch spacing. The effects of mass flow rate between the low and high levels of the pitch spacing are 16% and 13.81%, respectively. The interaction effect between (B × E) is ([13.81% − 16%]/2 = −1.09%). Here the highest effect of mass flow rate on efficiency is obtained at low level of the pitch spacing. Here again, the glazing temperature for a large spacing is sufficiently high that an increase in air mass flow rate cannot extract all the thermal energy available in this region, which led to higher radiative heat losses and in lower collector efficiency when compared to the increases in air mass flow rate for small spacing.

- Interactions between irradiation and mass flow rate (D × E)

Fig. 6(C) presents the interactions effect between irradiation and mass flow rate (D × E). This figure shows that going from the low to high level of irradiation, results in an efficiency reduction of 7.23% at low mass flow rate level compared to only 3.16% at high mass flow rate level. Increasing the flow rate decreases the drop of the efficiency due to the increase of irradiation level. Again, a high mass flow rate induces higher velocities through the absorber plate and the perforated glazing, which increases the heat transfer coefficient to the flowing air. In consequence, the equilibrium temperature of these surfaces decreases, which restrict the radiative losses from the TTC to the surroundings.

- Interactions between pitch spacing and slot width (B × C)

Fig. 6(D) shows the interaction effect between pitch spacing and slot width (B × C). The drop in efficiency due slot width increasing is more pronounced in case of perforated glazing with large pitch spacing (2.31%) compared to one of small slot spacing (0.91%). In other terms, it is by decreasing both the slot width and pitch spacing, we get the maximum efficiency. Such effects are due to the fact that, efficiency decreases slightly for low pitch spacing, because the temperature of the perforated glazing does not increases as much as in the case of a larger pitch spacing.

## 5. Conclusion and recommendation

Solar air heating systems are becoming more and more popular as they provide many possibilities for energy savings and for preheating air in various applications. In this context, the objective of the work presented here was to provide measurements from a reduced-scale prototype that can be used to estimate the thermal performance of TTCs and to study the influence of some design and operation parameters such as geometrical properties, irradiation, and air mass flow rate in terms of collector efficiency ($\eta_{coll}$). To determine these parameters effects, this experimental work used a multi level full factorial plan of replicated 48 tests.

The conclusions that can be drawn with the results of this investigation are of four orders:

First, using a multi-level factorial DoE, the effects of five preponderant parameters were evaluated in terms of the collector efficiency. All of the main effects are statistically significant as is the interaction between plenum thickness and slot width, interactions between pitch spacing and mass flow rate, interactions between irradiation and mass flow rate, and the interactions between pitch spacing and slot width. It was found that for the geometry, materials, and operating conditions used in this study, which are thought as being representative of TTC systems, that the efficiency is strongly dependent of the air mass flow rate. The effects of irradiation, slots width, pitch spacing, plenum thickness seem to be limited. The interactions between factors are not very pronounced, the strongest interaction is between plenum thickness and slot width.

Second, the analysis of main effects revealed that the efficiency of the TTC is moderately affected by the plenum thickness. Further investigations should be undertaken in the future using TTC's plenums with larger heights to assess the effect of this parameter. Pressure drop investigation should also be considered as the extra fan power to overcome pressure drop should be decreased from the gains to obtain the "net" efficiency.

Third, the analysis of interaction between the studied parameters revealed the importance of radiation heat exchanges to the heat transfer mechanisms between TTC surfaces component and surroundings. The radiative heat losses affect the thermal efficiency of the TTC and depends on solar and infrared performance properties of various TTC surfaces component, namely the absorber plate properties ($\alpha_{abs}$ and $\varepsilon_{abs}$) and the perforated glazing properties ($\varepsilon_g$ and $\tau_{ir,g}$). This may be a topic for future investigation.

Finally, the present investigation provides a data basis for a two-dimensional reduced scale model from which a detailed numerical study can be performed in the future. This allows extending the present work to the flow and heat transfer through the TTC.

## Acknowledgements

Financial support for this study was provided by the t3e industrial research chair and its financial partners; the authors would like to acknowledge their invaluable contributions. The authors wish to thank the laboratory of analytical chemistry of Université de Montréal and the solar energy and lighting laboratory of Concordia University for their help in the measurement of optical properties of glazing.

## References

[1] A.I. Kudish, E.G. Evseev, G. Walter, T. Leukefeld, Simulation study of a solar collector with a selectively coated polymeric double walled absorber plate, Energy Conversion and Management 43 (2002) 651–671.
[2] G. Martinopoulos, D. Missirlis, G. Tsilingiridis, K. Yakinthos, N. Kyriakis, CFD modeling of a polymer solar collector, Renewable Energy 35 (2010) 1499–1508.
[3] H. Tabor, H. Zeimer, Low-cost focussing collector for solar power units, Solar Energy 6 (1962) 55–59.
[4] A. Whillier, Plastic covers for solar collectors, Solar Energy 7 (1963) 148–151.
[5] R. Raman, S. Mantell, J. Davidson, C. Wu, G. Jorgensen, A review of polymer materials for solar water heating systems, Journal of Solar Energy Engineering 122 (2000) 92.
[6] A. Blaga, Use of plastics in solar energy applications, Solar Energy 21 (1978) 331–338.
[7] D. Njomo, Techno-economic analysis of a plastic cover solar air heater, Energy Conversion and Management 36 (1995) 1023–1029.
[8] D. Njomo, Modelling the heat exchanges in a solar air heater with a cover partially transparent to infrared radiation, Energy Conversion and Management 31 (1991) 495–503.
[9] O.V. Ekechukwu, B. Norton, Review of solar-energy drying systems III: low temperature air-heating solar collectors for crop drying applications, Energy Conversion and Management 40 (1999) 657–667.
[10] C. Balocco, M.A. Forastiere, G. Grazzini, G.C. Righini, Experimental results of transparent, reflective and absorbing properties of some building materials, Energy and Buildings 33 (2001) 563–568.
[11] G. Oreski, D. Tscharnuter, G.M. Wallner, Determination of solar optical properties of transparent polymer films using UV/vis spectroscopy, Solar Energy Materials and Solar Cells 94 (2010) 884–891.
[12] G. Oreski, D. Tscharnuter, G.M. Wallner, Development of methods to determine the infrared-optical properties of polymer films, Macromolecular Symposia 265 (2008) 124–133.
[13] M. Köhl, G. Jorgensen, S. Brunold, B. Carlsson, M. Heck, K. Möller, Durability of polymeric glazing materials for solar applications, Solar Energy 79 (2005) 618–623.

[14] G.M. Wallner, R.W. Lang, Aging of polymeric films for transparent insulation wall applications, Solar Energy 79 (2005) 603–611.
[15] X. Han, X. Zhang, Experimental study on a residential temperature–humidity separate control air-conditioner, Energy and Buildings 43 (2011) 3584–3591.
[16] I. Jaffal, C. Inard, C. Ghiaus, Fast method to predict building heating demand based on the design of experiments, Energy and Buildings 41 (2009) 669–677.
[17] V. Khalajzadeh, G. Heidarinejad, J. Srebric, Parameters optimization of a vertical ground heat exchanger based on response surface methodology, Energy and Buildings 43 (2011) 1288–1294.
[18] M. Badache, S. Hallé, D. Rousse, A full 34 factorial experimental design for efficiency optimization of an unglazed transpired solar collector prototype, Solar Energy 86 (2012) 2802–2810.
[19] K. Gawlik, C. Christensen, C. Kutscher, A numerical and experimental investigation of low-conductivity unglazed, transpired solar air heaters, Journal of Solar Energy Engineering 127 (2005) 153–155.
[20] J. Goupy, Pratiquer les plans d'expériences, Dunod, Paris, 2005.
[21] D.C. Montgomery, Design and Analysis of Experiments, 7th ed., John Wiley & Sons Inc, 2008.
[22] R.H. Myers, D.C. Montgomery, C.M. Anderson-Cook, Response Surface Methodology: Process and Product Optimization Using Designed Experiments, 3rd ed., John Wiley & Sons Inc, 2009.
[23] A. Pappas, Z. Zhai, Numerical investigation on thermal performance and correlations of double skin façade with buoyancy-driven airflow, Energy and Buildings 40 (2008) 466–475.
[24] A. Guardo, M. Coussirat, E. Egusquiza, P. Alavedra, R. Castilla, A CFD approach to evaluate the influence of construction and operation parameters on the performance of Active Transparent Façades in Mediterranean climates, Energy and Buildings 41 (2009) 534–542.
[25] M. Badache, D.R. Rousse, S. Hallé, G. Quesada, Experimental and numerical simulation of a two-dimensional unglazed transpired solar air collector, Solar Energy 93 (2013) 209–219.
[26] C.F. Kutscher, Heat exchange effectiveness and pressure drop for air flow through perforated plates with and without crosswind, Journal of Heat Transfer 116 (1994) 391–399.
[27] C. Choudhury, H.P. Garg, Design analysis of corrugated and flat plate solar air heaters, Renewable Energy 1 (1991) 595–607.
[28] G. Baillargeon, Probabilités, statistique et techniques de régression, Québec, SMG, 1989.
[29] G.F. Tjandraatmadja, L.S. Burn, M.C. Jollands, Evaluation of commercial polycarbonate optical properties after QUV-A radiation—the role of humidity in photodegradation, Polymer Degradation and Stability 78 (2002) 435–448.
[30] G. Oreski, G. Wallner, Structure-infrared optical property-correlations of polar ethylene copolymer films for solar applications, Solar Energy Materials and Solar Cells 90 (2006) 1208–1219.
[31] F.P. Incropera, T.L. Bergman, A.S. Lavine, D.P. DeWitt, Fundamentals of heat and mass transfer, 7th ed., John Wiley, 2011.
[32] A. Trombe, J.A. Moreau, Surface temperature measurement of semi-transparent material by thermocouple in real site experimental approach and simulation, International Journal of Heat and Mass Transfer 38 (1995) 2797–2807.
[33] Z. Chen, P. Bandopadhayay, J. Halldorsson, C. Byrjalsen, P. Heiselberg, Y. Li, An experimental investigation of a solar chimney model with uniform wall heat flux, Building and Environment 38 (2003) 893–906.
[34] S. Burek, A. Habeb, Air flow and thermal efficiency characteristics in solar chimneys and Trombe Walls, Energy and Buildings 39 (2007) 128–135.
[35] M. Sandberg, B. Moshfegh, Investigation of fluid flow and heat transfer in a vertical channel heated from one side by PV elements, Part II—Experimental study, Renewable Energy 8 (1996) 254–258.
[36] STATGRAPHICS Centurion XV, Statgraphics Centurion XV, 2009.
[37] C.F. Kutscher, An investigation of heat transfer for air flow through low-porosity perforated plates, University of Colorado at Boulder, 1992 (Ph.D. Thesis).